PCCP

Accepted Manuscript




ROYAL SOCIETY OF CHEMISTRY

www.rsc.org/pccp

# Robust Magnetic Domains in Fluorinated $ReS_2$ Monolayer

**G.C. Loh [a,b*], Ravindra Pandey [a,*]**

[a]Department of Physics, Michigan Technological University, Houghton, Michigan 49931, USA
[b]Institute of High Performance Computing, 1 Fusionopolis Way, #16-16 Connexis, Singapore 138632

(June 8, 2015)

**Email:**
G. C. Loh (jgloh@mtu.edu)
Ravindra Pandey (pandey@mtu.edu)

## Abstract

Transition metal dichalcogenides are layered materials that are typically bound together by van der Waals forces. An exception in the family is $ReS_2$; the geometrical distortion of its lattice structure due to Peierls distortion dimerizes Re atoms to form zigzag chains, thus decoupling the layers electronically and vibrationally. This in turn reduces the layer dependence of its physical and chemical properties. In order to tailor the properties of $ReS_2$ monolayer, an alternative way by fluorination above and between Re chains in the lattice is investigated. The results of density functional theory calculations show the site-dependent electronic properties of fluorinated $ReS_2$: (i) F atoms above the Re chains induce metallic mid-gap states which are ferromagnetically-coupled within the Re chains, and antiferromagnetically-coupled between chains; (ii) F atoms between the Re chains induce semiconducting mid-gap states which are non-magnetic. Unlike other states observed, the mid-gap states associated with top sites above the Re chains are generally insusceptible to the external electric field. The electron localization and negative Laplacian plots show that not only bonds between F and S atoms are ionic in character, the Re chains are also coupled ionically. The emergence of these robust metallic mid-gap states in the localized domains suggest that electrons could conduct along the Re chains by hopping. The electron conduction in such functionalized $ReS_2$ is anisotropic in nature, and hence could be applied in spintronic devices, such as spin-transfer torque and spin-wave logic devices.

Keywords: transition metal dichalcogenide, rhenium disulphide, mid-gap states, ferromagnetism

## 1. Introduction

The experimental discovery of graphene [1], and subsequent theoretical studies [2-6] on the plausibility of its integration in next-generation electronic applications triggered a re-examination of a particular category of graphene-like materials – transition metal dichalcogenides (TMDs). A few members of this class of materials are not novel; for instance, the superconducting nature of alkali-metal intercalates of molybdenum disulphide ($MoS_2$) was investigated many decades ago [7], while the van der Waals interaction between layers in bulk $MoS_2$ established it to be an excellent lubricant [8]. However the extent of scientific interest in TMDs during these years was relatively insignificant compared to that shown in graphene. It is the emergence of graphene, and the cornucopia of promising electronic functionalities it has presented that caused a paradigm shift in the importance of TMDs. Indeed, recent studies on $MoS_2$ have revealed its unique, intriguing, and yet functional electrical properties, including a large carrier mobility [9], and high current-carrying capacity [10], which rival those of graphene. Similarly, tungsten-based dichalcogenides such as tungsten disulphide ($WS_2$) and tungsten diselenide ($WSe_2$) have exhibited excellent electrical performance, and thus considered as alternative materials to graphene for device applications [11,12].

TMDs have a close resemblance to graphene due to their layered geometry, and hexagonal crystal structure. They are binary in composition with the chemical formula $MX_2$, whereby $M$ is a transition metal (e.g. $Mo, W, Ni, V, Re$), and $X$ is a chalcogen element (e.g. $S, Se, Te$) [13]. These atoms are stacked in a $X$-$M$-$X$ sandwich-like arrangement, i.e. a monolayer of TMD is composed of 3 sub-layers of atoms. There are primarily two phases of the material in its monolayer form; the hexagonal $(H)$ phase in which the $M$ layer is trigonal and prismatic with respect to the $X$ layers, while in the octahedral $(T)$ phase, the $X$ layers are ordered in a staggered manner forming octahedral holes for $M$ atoms. Apart from the $H$ and $T$ phases, other phases include the rutile, pyrite, and marcasite phases, of which a few TMDs can exist in the three-dimensional (3D) bulk form [13]. A common characteristic of TMDs such as $MoS_2$, molybdenum diselenide ($MoSe_2$), $WS_2$, and $WSe_2$ is the indirect-to-direct

band gap transition, and an increase of the band gap due to strong interlayer coupling and out-of-plane carrier confinement with the reduction of the number of layers from the bulk to a single layer [14-19]. Moreover, the electronic band structure can be tuned by mechanically straining the lattice structure of monolayer TMDs, either by applying an external biaxial tensile strain [20], or via lattice mismatch with a substrate [21]. Therefore the electronic properties of TMDs can be tailored to suit different applications, and thereby extending their functionalities for next-generation devices.

In general, the layer-dependent electronic properties is not always found to be desirable for applicability of a given electronic material; inconsistencies and imperfection of synthesis techniques pose challenges in controlling the number of layers in the material, and hence often lead to a large variance in electronic properties within different samples. Such a problem has been predicted to be averted in rhenium disulphide ($ReS_2$). It is a relatively new member of the group-VII TMD family with partially filled 3d-shell [22]; its synthesis [23,24] and implementation in field-effect transistors (FETs) [25] has only been reported recently. In multilayer $ReS_2$, the intralayer Re-S bonds are covalent, while the interaction between layers is weak and of the van der Waals (vdW) type. In stark contrast to many other TMDs, its 1T phase undergoes Peierls distortion to form buckled S layers, with dimerization of Re atoms to form zigzag chains. As a result, each layer becomes electronically and vibrationally decoupled from the others in the distorted $CdCl_2$-type structure; in fact, density functional theory (DFT) calculations predict a interlayer coupling energy of only ~18 meV per unit cell, which is approximately 8% of the interlayer coupling energy of $MoS_2$ [23]. Despite the weak interlayer forces in both $ReS_2$ and $MoS_2$, the existence of different polytypes is found only in the latter [26-28], whereas the only stable form $ReS_2$ can exist in is the distorted octahedral phase. Due to the interlayer decoupling, both bulk and monolayer $ReS_2$ are predicted to have nearly identical band structures in the DFT calculations. Both are semiconductors with a direct band gap of 1.35 eV, and 1.43 eV [23] (or 1.47 eV in Ref **29**), respectively. The decoupling between layers has been confirmed by high-resolution transmission electron microscopy (HRTEM) and electron diffraction experiments [23]. In addition, the

optical absorption and Raman spectra of the material are impervious to a modulation of interlayer coupling by external hydrostatic pressure [23]. The weak contingency of the electronic properties of $ReS_2$ on the number of layers essentially alleviates the tricky problem of controlling the thickness of the material during growth.

Thickness control is just one of the many methods to engineer the electronic properties of TMDs. Alternatives include incorporation of dopants [30], and decoration of the surface or edges with adatoms. In the latter, for instance, it has been reported that partial edge hydrogenation of armchair $MoS_2$ nanoribbons converts them from a semiconductor to a metal/semimetal under a moderate external transverse electric field. Moreover, localized ferromagnetic (FM) states are induced at the edges [31]. Similarly, adding hydrogen to the edges of armchair $WS_2$ nanoribbons invokes drastic changes to its band structure, and transforms them into a magnetic semiconductor [32]. In other 2D materials such as graphene and boron nitride (BN) monolayer, chemical functionalization of the surface with adatoms such as hydrogen and fluorine has been demonstrated to be an effective way of manipulating spin transport, and hence making these viable materials for spintronics applications [33,34].

Reducing the dependence of the electronic properties of a material on its thickness makes the synthesis process simpler and easier, but if the properties of the material can be tailored, a greater scope of applications then becomes a possibility. In view of the efficacy of chemical functionalization in band gap and spin engineering of materials, we might ask: can we use this approach to modify the electronic characteristics of $ReS_2$? Since the adsorption of fluorine has been shown to moderate the electronic and magnetic properties of two-dimensional layered materials [33,34], it is of interest to investigate its effects on these properties of $ReS_2$. Due to the unique distorted geometry of the material with dimerization of Re atoms to form zig-zag chains, the electronic and magnetic response might be dissimilar at different regions of the material. In particular, it is imperative to compare these effects invoked by adsorption of fluorine atoms above the Re chains, and between two chains in the $ReS_2$ monolayer. In this study, these effects are investigated using density functional theory. Section 2

gives the details of the computational model, and results are discussed in Section 3. Section 4 draws a conclusion, highlighting the most important results of this work.

## 2. Computational Model

The monolayer $ReS_2$ is simulated by a (4 × 4) supercell containing 16 Re and 32 S atoms. The atoms are arranged in a distorted octahedral manner with a Re sub-layer sandwiched between two S sub-layers. F atoms are then deposited on top the upper sub-layer of S atoms. In the ground state configuration, the Re-S bond length ranges from 2.33 to 2.48 Å, while the Re-Re bond length in the zig-zag chains ranges from 2.68 to 2.88 Å. Note that our calculated Re-S and Re-Re bond lengths compare well with experimental values of around 2.38 Å and 2.69 - 2.82 Å, respectively [35]. The separation between sub-layers is approximately 1.48 Å. The formation energy of pristine monolayer $ReS_2$ with respect to its constituents is calculated to be -5.79 eV/atom.

Next, seven main configurations of fluorine on $ReS_2$ are considered for calculations: (1) 4 F atoms above Re chains at Position A *[4 F@Above A]* (Figure 1(a)), (2) 4 F atoms above Re chains at Position B *[4 F@Above B]* (Figure 1(b)), (3) 4 F atoms below Re chains at Position C *[4 F@Below C]* (Figure 1(c)), (4) 4 F atoms below Re chains at Position D *[4 F@Below D]* (Figure 1(d)), (5) 2 F atoms above Re chains at Position A *[2 F@Above A]* (Figure 1(e)), (6) 4 F atoms between two Re chains *[4 F@Bet]* (Figure 1(f)), and (7) 2 F atoms between two Re chains *[2 F@Bet]* (Figure 1(g)). As a point of reference, another configuration is also considered - F atoms adsorbed above Re chains at Positions A, B, and below Re chains at Positions C, D *[F@A,B,C,D]* (Figure 1(h)). Due to symmetry, a smaller (1 × 1) cell is sufficient for *[F@A,B,C,D]*. Essentially, these configurations are selected to investigate and contrast how (i) adsorption at four different locations along the Re chains (*[4 F@Above A], [4 F@Above B], [4 F@Below C] and [4 F@Below D]* ), (ii) the surface coverage of $ReS_2$ with F atoms (*[4 F@Above A]* with coverage at all sites similar to Position A and *[2 F@Above A]* with half the

coverage at sites similar to Position B) ; *[4 F@Bet]* and *[2 F@Bet]*), and (iii) adsorption above the Re chain and between 2 Re chains (*[4 F@Above A]* and *[4 F@Bet]*), affect the modification of the electronic and magnetic properties of the material, if any. We find that F atoms always relax to be positioned above or below the S layers, i.e. Re atoms in $ReS_2$ do not bind with F atoms. Hence, only configurations with F atoms adsorbed on S atoms have been considered for the remaining calculations.

The adsorption sites above Position A (*[4 F@Above A]*) and below Position C (*[4 F@Below C]*) are essentially identical, and the same is true for Positions B (*[4 F@Above B]*) and D (*[4 F@Below D]*). This is then verified by the calculated energies of these configurations. Therefore, only *[4 F@Above A]* and *[4 F@Above B]* are considered for the rest of the calculations. To test the stability, the dynamical matrix is calculated to derive the vibrational frequencies of the five main configurations (Figure S1, See Supporting Information). We note that *[4 F@Above B]* has an imaginary eigen-frequency at approximately -25 $cm^{-1}$, which is sufficiently small, and is likely to be due to numerical approximations including the particular convergence criterion employed. Therefore we expect fluorinated $ReS_2$ to be stable.

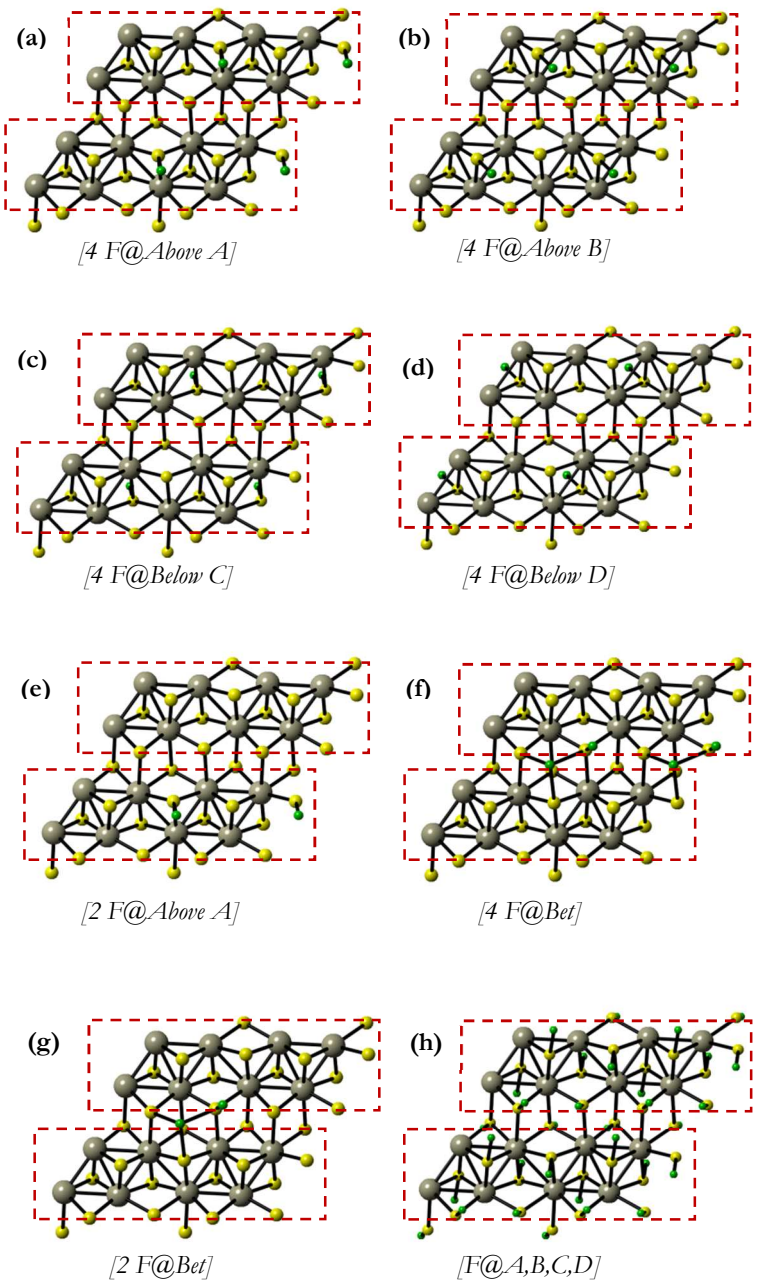


*Figure 1. Top views of $ReS_2$ with (a) 4 F atoms adsorbed above Re chains at Position A, i.e. [4 F@Above A], (b) 4 F atoms adsorbed above Re chains at Position B, i.e. [4 F@Above B], (c) 4 F atoms adsorbed below Re chains at Position C, i.e. [4 F@Below C], (d) 4 F atoms adsorbed below Re chains at Position D, i.e. [4 F@Below D], (e) 2 F atoms adsorbed above Re chains at Position A, i.e. [2 F@Above A], (f) 4 F atoms adsorbed between Re chains,*

*i.e. [4 F@Bet], (g) 2 F atoms adsorbed between Re chains, i.e. [2 F@Bet], and (h) F atoms adsorbed above Re chains at Positions A, B, and below Re chains at Positions C, D, i.e. [F@A,B,C,D]. Atoms in grey are Re, yellow are S, and green are F. The dashed boxes marked the Re chains.*

Calculations based on density functional theory (DFT) were performed with the VASP (Vienna Ab Initio Simulation Package) program, and the implementation of projector augmented-wave (PAW) pseudopotentials [36] (with an energy cutoff of 400 eV). The Perdew-Burke-Ernzerhof (PBE) exchange-correlation functional in the generalized gradient approximation (GGA) [37] was used. Dispersion correction was included in the calculations by the DFT-D3 approach of Grimme [38]. The Brillouin zone was sampled with a (19×19×1) k-point mesh using the Monkhorst-Pack scheme [39]. The structures were optimized until the forces (as calculated by the Hellmann-Feynman formalism [40,41]) were less than $10^{-5}$ eV/Å.

In the calculations, the (4×4) supercell is separated from its periodic image in the direction perpendicular to the surface by a vacuum region of 12 Å. Dipole corrections were applied in the direction perpendicular to the material surface to avoid interactions between periodically repeated images. Spin-orbit interactions were considered initially, and the total energy difference between calculations with and without these interactions is ≈ 0.14 eV/atom. Furthermore, the relatively trivial effects of spin-orbit interactions on the band structure (elaborated further in Section 3.2) justifies the exclusion of these interactions in the calculations in order to employ our modest computing resources more effectively.

To partition the continuous charge density among the atoms in the system, Bader's atoms in molecules theory [42-46] is implemented, such that the atomic basin is determined at the zero flux surface around the atom. This surface is observed in the two-dimensional sense at which the charge

density is at a minimum perpendicular to the system surface. Therefore the total electronic charge of each atom can be defined.

## 3. Results and Discussion

### 3.1 Fluorinated $ReS_2$: Band Structure & Charge Density

The atom-projected electronic band structures of pristine and fluorinated $ReS_2$ are given in Figure 2. For the pristine $ReS_2$, the valence band is almost flat in the vicinity of Γ since the spin-orbit interactions shift the valence band maximum (VBM) from a point along Γ-K or Γ-M direction to Γ [47]. However the direct (Γ → Γ) and indirect (ΓK → Γ; ΓM → Γ) band gaps in the pristine $ReS_2$ (Figure 2(a)) and *[2 F@Above A]* (Figure 2(d)) are almost degenerate in energy (difference ≈ 10 meV). Thus, the valence band maximum (VBM) is taken to be at Γ for the cases of pristine and *[2 F@Above A]* $ReS_2$. On the other hand, the energy difference between direct and indirect band gaps is slightly larger (≈ 40 meV) for the case of *[4 F@Above A]* (Figure 2(b)). In this case, we take VBM to be between Γ and M. Nevertheless, the modeling elements employed in our work do not alter the electronic behavior, as it would be explained later.

With that put forth, we find that the pristine $ReS_2$ has a direct band gap of 1.40 eV at Γ (Figure 2(a)), which agrees well with that in Ref **23** (1.43 eV) and **29** (1.47 eV). Addition of 4 F atoms above the Re chains at Position A *[4 F@Above A]* induces metallic mid-gap states with a band-width of 0.50 eV (Figure 2(b)). These mid-gap states are associated with electronic states of Re, S, and F atoms. The occupied states shift towards a higher energy as compared to those of the pristine $ReS_2$, and remain generally invariant in their trend. On the other hand, the unoccupied bands shift towards a lower energy, and the conduction band minimum (CBM) relocates from Γ to K. Since the electronic behavior of *[4 F@Above A]* is dominated by the metallic mid-gap states, the slight shift of VBM due to the exclusion of spin-orbit interactions becomes inconsequential. In comparison, adding F atoms

above the Re chains at Position B *[4 F@Above B]* shifts the occupied states more towards a higher energy relative to that when F atoms are at Position A (Figure 2(c)). Similarly, the unoccupied states shift towards a higher energy. Both VBM and CBM remain at Γ. The mid-gap states form 4 bands with a band-width of about 0.33 eV for the case of *[4 F@Above B]*. As a comparison, adsorbing F atoms at Positions A, B, C, and D, i.e. *[F@A,B,C,D]*, induce metallic states with a much larger band-width of approximately 1.10 eV (Figure 2(g)).

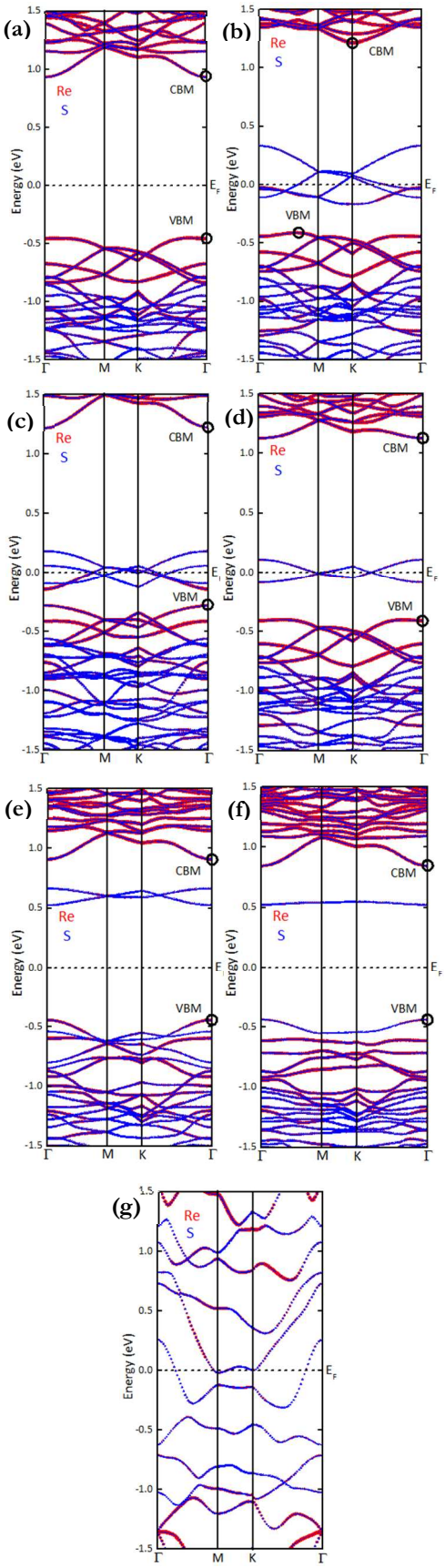

*Figure 2. Atom-projected band structure of (a) pristine $ReS_2$, (b) [4 F@Above A], (c) [4 F@Above B], (d) [2 F@Above A], (e) [4 F@Bet], (f) [2 F@Bet], (g) [F@A,B,C,D]. Points in red and blue refer to contribution from Re and S atoms, respectively. The size of the data points indicates the spectral weight. Zero is taken to be Fermi energy.*

Why does fluorination of $ReS_2$ induce mid-gap states? Here we shall explain in terms of the Bader charges. In pristine $ReS_2$, each S atom is bonded to 3 Re atoms. Re has an electron configuration of $[Xe]4f^{14}5d^{5}6s^{2}$ and S has an electron configuration of $[Ne]3s^{2}3p^{4}$; each Re and S atom has 5 unpaired 5d electrons and 2 unpaired 3p electrons, respectively. As F atom is more electronegative than S atom (F: 3.98, S: 2.58 by Pauling [48]), F tends to attract electrons from S. In fact, for *[4 F@Above A]*, Bader's charge analysis [42-46] shows that S loses 0.50 e/atom, F gains 0.52 e/atom, and the surrounding three Re atoms gain 0.02 e/atom. This suggests that F gains some charges from neighboring atoms other than S it is bonded to. Apparently, by bonding F to S, the S atom loses electrons to F. Consequently, the electron-deficient 3p electrons of S are partially satisfied by the 2p electrons of F (electron configuration: $[He]2s^{2}2p^{5}$), leaving behind some unpaired 3p electrons which emerge as mid-gap states. Similarly, the neighboring Re atoms gain some electrons, but some of the 5d orbitals remain unpaired, appearing as mid-gap states in the band structure.

The orbital-projected band structure (Figure 3(a)) and the band-decomposed charge density landscape (Figures 4 and 5) reveal the nature of the electronic states more clearly. As shown in Figure 3(a), the mid-gap states mainly comprise of F-$p_z$, Re-$d_{xz}$, and S-$p_z$ states. Note that contributions from other states are not presented since they are much less significant than those of F-$p_z$, Re-$d_{xz}$, and S-$p_z$. The mid-gap states at Γ localized around the F atoms are p-orbital-like with 1 angular node and 2 large lobes aligned along the F-S bond (Figure 4(b), and inset). However, radial nodes are not discernible from the charge density plot. The mid-gap states around the S atom and neighboring three Re atoms match closely to p-electrons (1 angular node, 2 large nodes) and d-electrons (2 angular nodes, 4 large lobes), respectively. Akin to the states at the F atom, radial nodes are not

distinct. On the other hand, the states at CBM are localized around every Re atom. They have d-orbital character due to their 4 large lobes (Figure 4(b)). In contrast, the states at VBM are located around Re atoms in alternating diagonal rows. The states at CBM and VBM primarily originate from the Re atoms (Figure 2b)). Essentially, the emergence of localized metallic mid-gap states near the Fermi level suggest that hopping conduction of the states is possible along the Re chain in the lattice [49-57].

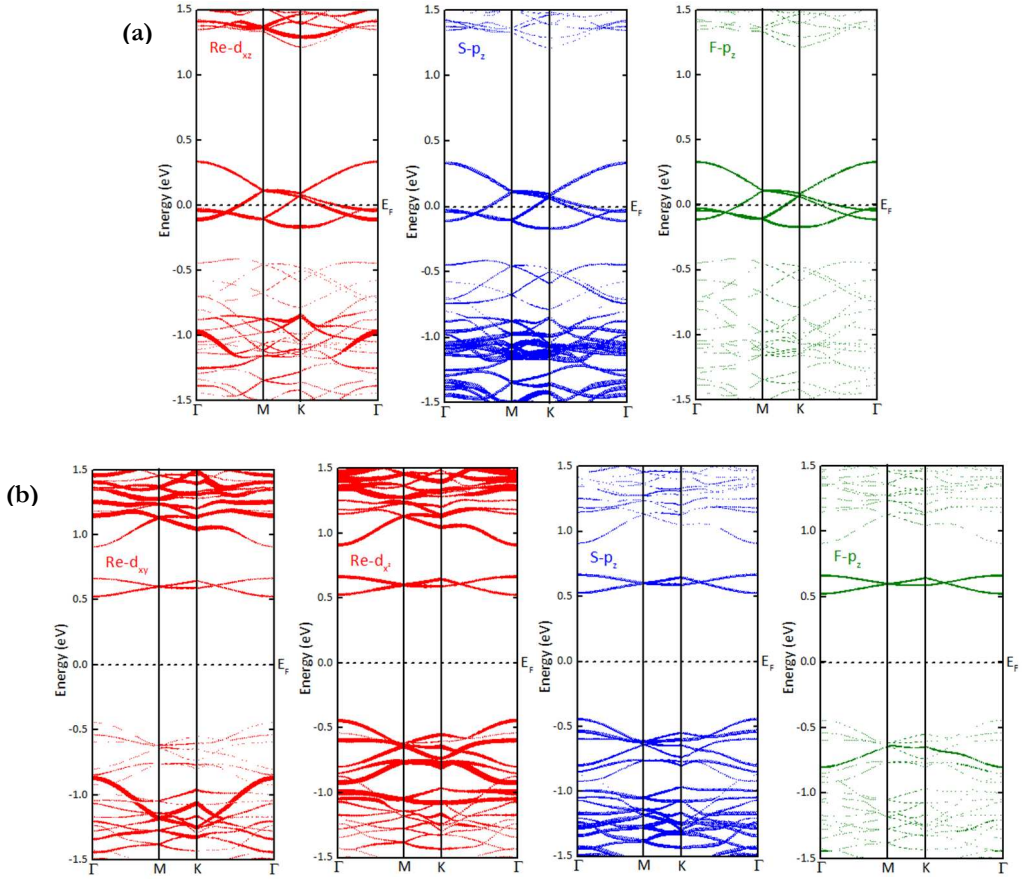


*Figure 3. (a) Orbital-projected band structure of (a) Re-$d_{xz}$, Re-$p_z$, F-$p_z$ states of [4 F@Above A], and (b) Re-$d_{xy}$, Re-$d_{x2}$, S-$p_z$, F-$p_z$ states of [4 F@Bet]. The size of the data points indicates the spectral weight. Zero is taken to be Fermi energy.*

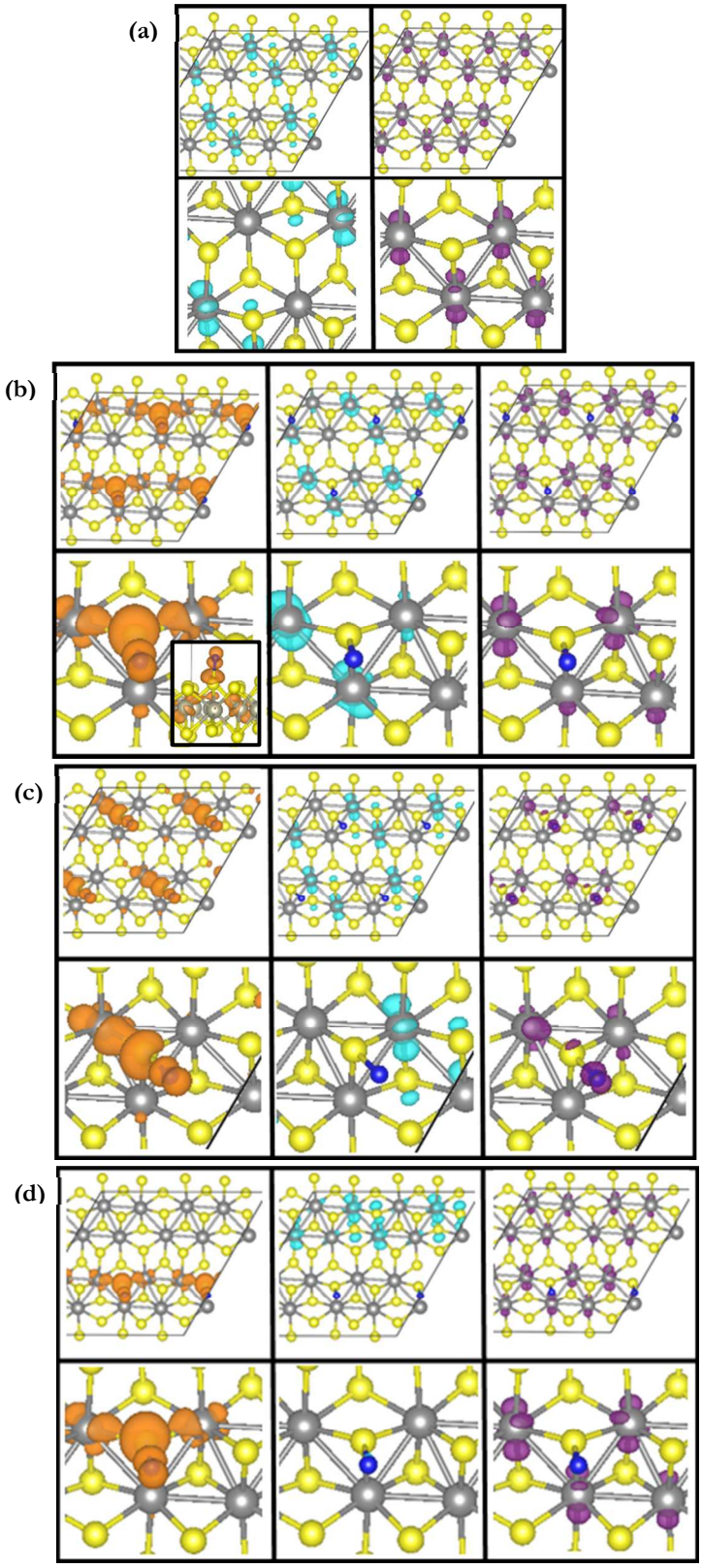

*Figure 4. Top views of the partial charge density landscape of (a) pristine $ReS_2$, (b) [4 F@Above A], and (c) [4 F@Above B], (d) [2 F@Above A]. The regions in orange, cyan, and purple refer to the charge density of mid-gap states at Γ, CBM, and VBM, respectively. The contour isovalue is 0.01, 0.005, and 0.005 e/Å³ for mid-gap states, CBM, and VBM, respectively. The bottom panels are magnified views of one of the fluorinated regions, while the inset in (b) is the side view.*

Similar to *[4 F@Above A]*, the mid-gap states in *[4 F@Above B]* (Figure 4(c)) are localized around the F atom, the neighboring S and Re atoms. In these localized domains, the character of the charge distribution, including the shape of lobes, and the number of lobes and nodes suggest that these states are the p states of the S, F atoms, and the d states of the Re atoms. With less F atoms adsorbed on $ReS_2$ at Position A, i.e. *[2 F@Above A]*, the occupied and unoccupied states generally remain unchanged, except for a slight shift towards a higher energy (Figure 2(d)). Two bands of metallic mid-gap states are induced, and have a band-width of around 0.20 eV which is smaller than that of *[4 F@Above A]*. VBM and CBM are located at the Γ. The charge distribution of the mid-gap states at Γ, and VBM resemble that of *[4 F@Above A]* (Figure 3(d)). However, the states at CBM are localized around Re atoms on the neighboring Re chain, and not around all Re atoms.

When F atoms are placed in the regions between Re chains (*[4 F@Bet], [2 F@Bet]*), mid-gap states above the Fermi level appear (Figures 2(e) and (f)). There are slight changes to the occupied bands, especially for those near the top of the valence band, whereas the unoccupied bands generally remain unchanged. Due to the emergence of the semiconducting mid-gap states, the band gap is reduced from 1.40 eV to 0.97 eV for *[4F@Bet]* and 0.96 eV for *[2F@Bet]*, but remain direct at the Γ. Akin to the metallic mid-gap states, these semiconducting states originate mainly from both Re and S atoms, but with a smaller band-width of 0.14 eV and 0.03 eV for *[4F@Bet]* and *[2F@Bet]*, respectively. The spatial distribution of the semiconducting mid-gap states is disparate from their metallic counterparts (Figures 5(a) and (b)); the mid-gap states are primarily localized around the S and F atoms. There are

two types of F-S bonds; the first type is such that the F atom is bonded directly above a S atom, whilst in the other, the F atom is bonded to 3 neighboring S atoms. In both configurations, the mid-gap states are predominantly localized around the S atom in the first type of F-S bond. Figure 3(b) shows that these mid-gap states are mainly from the Re-$d_{xy}$, Re-$d_{x2}$, S-$p_z$, and F-$p_z$ states, and the states at CBM and VBM are located at nearby Re and S atoms (Figure 5).

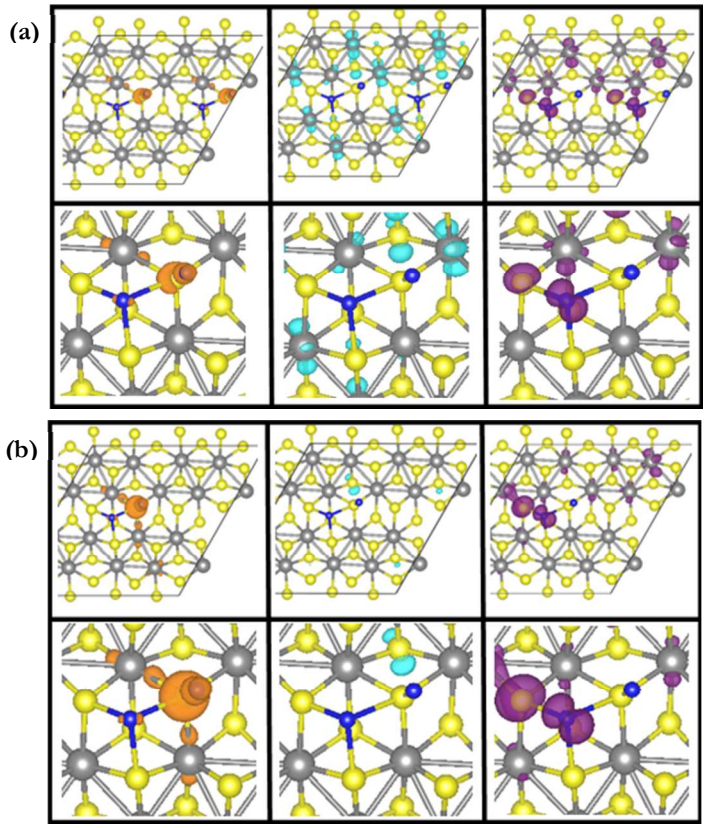


*Figure 5. Top views of partial charge density landscape of (a) [4 F@Bet], and (c) [2 F@Bet]. The regions in orange, cyan, and purple refer to the charge density of mid-gap states at Γ, CBM, and VBM, respectively. The contour isovalue is 0.01, 0.005, and 0.005 e/Å³ for mid-gap states, CBM, and VBM, respectively. The bottom panels are magnified views of one of the fluorinated regions.*

In *[F@A,B,C,D]*, the metallic states are localized around the F atom, the neighboring S and Re atoms, and are homogeneously distributed along the Re chains, particularly around the F atoms (Figure 6). Similarly, the character of the charge distribution, including the shape of lobes, and the number of lobes and nodes suggest that these states are the p states of the S, F atoms, and the d states of the Re atoms.

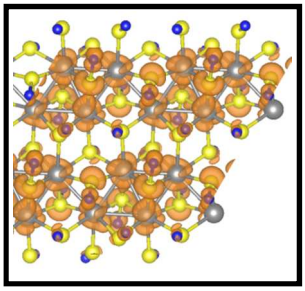

*Figure 6. Top view of partial charge density landscape of [F@A,B,C,D]. The regions in orange refer to the charge density of metallic states. The contour isovalue is 0.01 e/Å³.*

### 3.2 Fluorinated $ReS_2$: Spin Density

To investigate the preferred spin states of the fluorinated $ReS_2$ in its equilibrium configuration, calculations were performed for the non-magnetic, ferromagnetic (FM) and antiferromagnetic (AFM) spin configurations. In the non-magnetic state, the spin moment of each atom is initialized to be zero. We define the initial FM spin configuration to consist of parallel (↑↑) spins between all atoms, and an initial AFM spin configuration to consist of anti-parallel (↑↓) spins between neighboring atoms. Due to Peierls distortion to form Re zigzag chains, the bond connectivity around the chains is complex. Hence, there are numerous permutations of the AFM configuration, and it is not feasible to investigate all of them. Here we study three of the many possible initial AFM spin configurations

($AFM_1$, $AFM_2$, $AFM_3$). As presented later, *our calculations show that it is likely that there are only two possible equilibrium AFM configurations* – the first of which is (1) FM-coupled within the Re chains, and AFM-coupled between chains, and (2) AFM-coupled within the chains. Only the initial AFM spin configurations for *[4 F@Above A]* are shown in Figure S2 (Supporting information); for the other structures, the initial spins on each Re and S atom are identical to those in Figure S2, while the spin on the F atom is always aligned anti-parallel to that of its adjoining S atom.

In *[4 F@Above A]*, one of the configurations which relaxes from $AFM_1$ and $AFM_2$ is the most preferential. The total energy of the non-magnetic and FM configurations is higher by 0.08 eV and 0.07 eV, respectively, while the other AFM configuration has a total energy of 0.07 eV (relaxes from $AFM_3$). For the ground state, the spin density of *[4 F@Above A]* redistributes into domains of net spin density which are AFM-coupled between neighboring chains, and FM-coupled within the chains (Figure 7(a)). At the isovalue of 0.005 e/Å$^3$, the neighboring 2 Re atoms, S atom, and F atom have a net spin density – the regions in red have a larger spin-up density (i.e. $n_{up} - n_{down} > 0$), while those in blue have a larger spin-down density (i.e. $n_{up} - n_{down} < 0$). The Re atom (marked as Atom 1 in Figure 7(a)), S atom (Atom 2), and F atom (Atom 3) has a magnetization moment of 0.180, 0.144, and 0.153 $\mu_B$/atom, respectively. Note that both Re atoms (Atom 1) have the same magnetization moment. Similarly, the FM equilibrium configuration consists of domains which are FM-coupled intra- and inter-chain.

The spin-polarized band structure is presented in Figures S3(a) and (b) (Supporting Information). The mid-gap states undergo exchange splitting of around 0.2 eV, and both induced spin-up and spin-down mid-gap states are partially occupied.

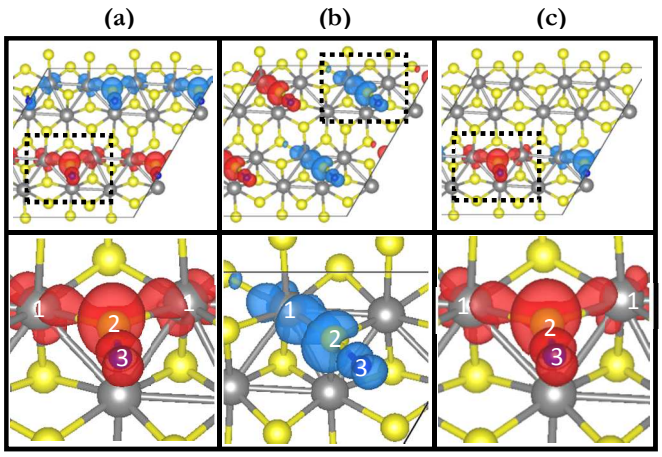


*Figure 7. Spin density distribution in the equilibrium configurations of (a) [4 F@Above A], (b) [4 F@Above B], and (c) [2 F@Above A]. The contour isovalue is 0.005 e/Å³. Regions in red have a net spin-up density, whereas those in blue have a net spin-down density. The bottom panels are magnified regions of the dotted regions in the top panels.*

For *[4 F@Above B]*, the most energetically preferential configuration is AFM-coupled within the chains (from $AFM_3$, Figure 7(b)). The Re, S, and F atom has a magnetization moment of 0.310, 0.149, and 0.174 $\mu_B$/atom, respectively. In the FM configuration, domains are FM-coupled intra- and inter-chain. The AFM configuration that relaxes from $AFM_1$ and $AFM_2$ is FM-coupled within the chains and AFM-coupled between chains. The total energy of the non-magnetic and FM configurations is larger than the ground state by 0.20 eV and 0.06 eV, respectively, while the other AFM configuration is at 0.05 eV. The spin-polarized band structure is shown in Figures S3(c) and (d); the spin-up and spin-down mid-gap states are partially occupied, with exchange splitting of about 0.2 eV, and all states are degenerate in energy levels. Although *[4 F@Above B]* has a larger magnetization moment than *[4 F@Above A]*, its total energy is slightly larger by approximately 0.01 eV. Assuming the absence of statistical errors, *[4 F@Above B]* could be less stable.

The domains of net spin density in *[2 F@Above A]* are AFM-coupled (from $AFM_3$) within the fluorinated chain. The $AFM_1$ configuration relaxes to be FM-coupled intra-chain. The magnetization moment of the ground state is slightly larger than that relaxed from $AFM_2$ of *[4 F@Above A]* at 0.128, 0.157, and 0.161 $\mu_B$/atom for the Re, S, and F atom, respectively. The total energy of the non-magnetic and FM configuration is 0.09 eV and 0.02 eV, with respect to the ground state, respectively. The spin-polarized bands near the Fermi level (Figures S3(e) and (f)) are almost flat, with exchange splitting of around 0.1 eV.

On the other hand, the configurations *[4 F@Bet]*, *[2 F@Bet]* and *[F@A, B, C, D]* have a non-magnetic ground state. In other words, for the former two, the localized mid-gap states induced by the F atoms adsorbed between Re chains are semiconducting (Figures 2(e), (f), and 5) and non-magnetic. Fluorination of the Re chains redistributes the spin density to induce a net spin density, whereas fluorination between the Re chains do not result in such an effect. This suggests that both the *electronic* and *magnetic* nature of the mid-gap states induced by fluorination on the surface of $ReS_2$ is strongly dependent on the coupling between the Re and F atoms in the lattice.

As reported in Ref **34**, BN sheets can be made ferromagnetic, antiferromagnetic, or magnetically degenerate depending on how the surface is functionalized. In contrast, fluorinated $ReS_2$ has an antiferromagnetic ground state, and its spin configuration is dependent on the sites on which the F atoms are adsorbed, and the number of F atoms adsorbed.

### 3.3 Electric Field Effects

The emergence of ferromagnetic mid-gap states in fluorinated $ReS_2$ widens its scope of applications. However, it is imperative to ascertain the robustness of these states, especially in the presence of external field. In other words, are these localized mid-gap states perceptible to external agitation, such as electric fields? Essentially, the force exerted by the electric field disturbs the electronic structure of

the material, and the degree of change deviates for different electronic states of the material. *In this study, we test and qualify the robustness of the mid-gap states by examining the response of these states to an external electric field.*

An electric field with its strength ranging from -0.7 to 0.7 eV/Å is applied in the direction perpendicular to the material surface. Figure 8(a)-(e) compares the band structure of the five main configurations when the electric field strength is at -0.7, 0, and 0.7 eV/Å. When F atoms are adsorbed at Position A, i.e. *[4 F@Above A]* and *[2 F@Above A]*, only bands far from the Fermi level are perturbed by the electric field, though there is no discernible trend in change of the energy levels with respect to the electric field. Interestingly, the mid-gap states are relatively resistant to the applied electric field, with very slight changes near the Γ. In contrast, the band structure of other configurations (*[4 F@Above B]*, *[4 F@Bet]*, and *[2 F@Bet]*) is significantly perturbed by the electric field. For instance, a small direct energy gap of 0.13 eV is opened up at M for an electric field strength of 0.7 eV/Å for *[4 F@Above B]* (Figure 8(b) inset).

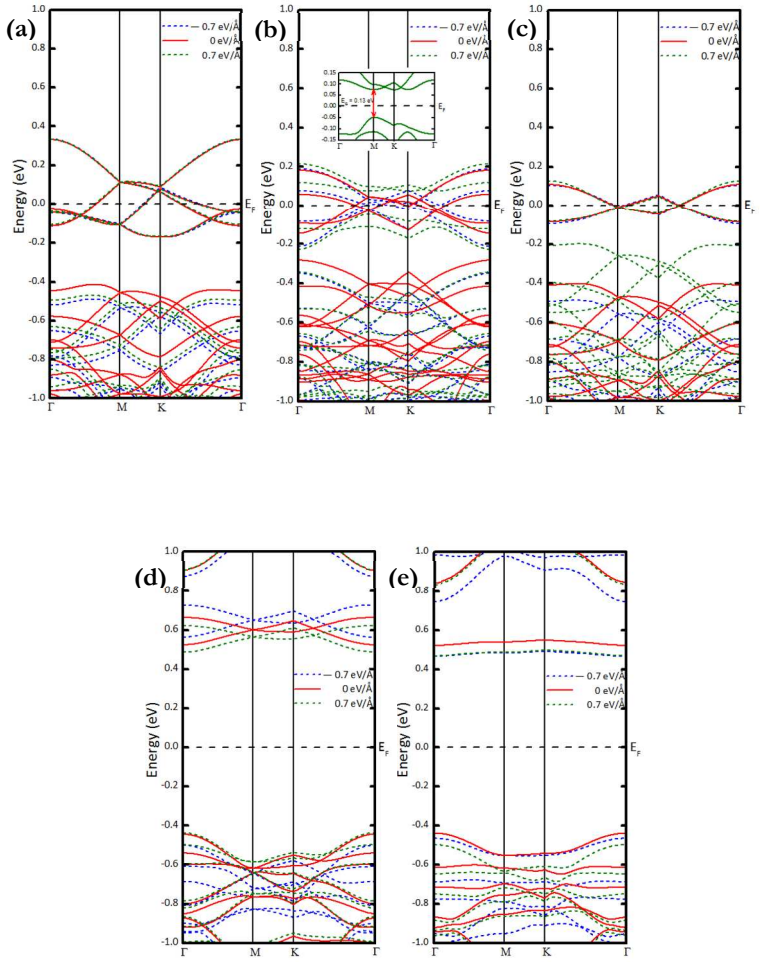


*Figure 8. (a) Band structure of (a) [4 F@Above A], (b) [4 F@Above B], (c) [2 F@Above A], (d) [4 F@Bet], and (e) [2 F@Bet] with an external electric field of -0.7, 0, and 0.7 eV/Å. Zero is taken to be Fermi energy.*

Additionally, the variation of the adsorbate binding energy $\Delta E_b$ with the electric field for all configurations is presented in Figure 9. The binding energy is expressed as

$$\Delta E = E_{F/ReS2} - E_{ReS2} - E_F \quad (1)$$

where $E_{F/ReS2}$, $E_{ReS2}$, and $E_F$ are the total energies of $ReS_2$ with F, without F, and of $ReS_2$ itself. Applying an electric field normal to the material surface in either direction enhances the binding energy of the F atom to the $ReS_2$ surface.

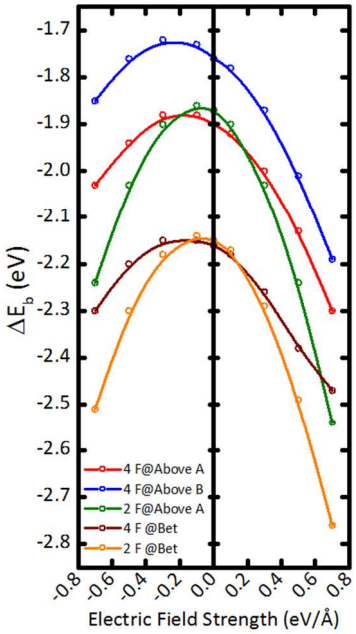


*Figure 9. Variation in the binding energy ($\Delta E_b$) of F to $ReS_2$ with the electric field strength.*

The change of the average magnetic moment of the magnetic domains with the electric field is shown in Figure 10. The average value is calculated from the magnetic moment of each atom in the localized magnetic domains. When F atoms are adsorbed at Position A (*[4 F@Above A]* and *[2 F@Above A]*), the magnetic moment is smaller in magnitude and much less sensitive to a variation of the field strength compared to the case in which the F atoms are adsorbed at Position B. This disparity in response to a variation of the field strength justifies what has been observed in Figures 8(a) and (c) – the mid-gap states induced by fluorinating Re chains at Position A are robust. Furthermore, the extent of contribution of Re and S atoms in the magnetic domains to the average

magnetic moment is presented by color-coding the data points in Figure 10. For all configurations, there is a reduction in contribution to the magnetic moment from Re and S atoms as the electric field switches from the negative to the positive regime; the decrease in contribution is smaller in *[4 F@Above B]*.

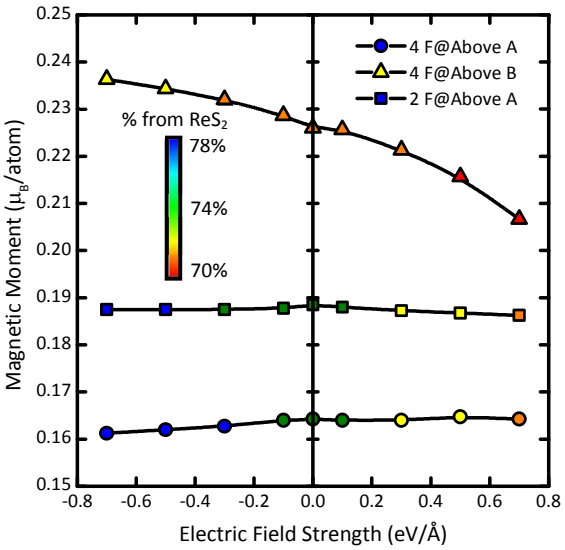


*Figure 10. Variation in the average magnetic moment of the localized domains with the electric field strength. The data points are colour-coded to reflect the contribution of the moment from $ReS_2$.*

### 3.4 Chemical Topology: Electron Localization Function & Laplacian Plots

Last but not least, we examine the nature of the chemical bonds, i.e. the chemical topology, in this two-dimensional material. The chemical bond, or more specifically, the electron density distribution between atoms can be described accurately by two tools - the first is the electron localization function ($ELF$) [58-60], and the second is the Laplacian of the electron density via the quantum theory of atoms in molecules [42-46]. The $ELF$ is a measure of the likelihood of finding an electron in the vicinity of a reference electron located at a particular point, with the same spin [61]. Mathematically

$$ELF = \left\{1 + \left[\frac{C(\vec{r})}{C_h(\rho(\vec{r}))}\right]^2\right\}^{-1} \quad (2)$$

where $\vec{r}$ is the radial distance from the nucleus, and $\rho$ is electron spin density. It ranges from 0 to 1, with it approaching 1 when r is within the pair region, and it is small when r is close to the border between two pair regions. In a homogeneous electron gas, the $ELF$ is 0.5 at every location. The covalency of the bond is primarily delineated by the form of the charge attractors; if they are more spherically distributed around the cores of the atoms, the interaction is more ionic or highly van der Waals in nature. In a more covalent bond, the attractor is more symmetric about the cores, while still lying on the bond line connecting the cores. The number and form of the localization regions are strongly dependent on the choice of the $ELF$ isovalue, and conventionally, an isovalue of approximately 0.80-0.85 is used for valence compounds.

The $ELF$ landscape is taken as a vertical 2D slice through the adsorbed F atom and the neighboring S atoms (Figure 11(a)-(c)). The localization region of isovalue 0.8 (represented in yellow in the plots) envelopes the nucleus of each atom aspherically, and is asymmetrical about the center point between any pair of F-S atoms. This suggests that the F-S bond is rather ionic in character. Moreover, plotting the 2D $ELF$ landscape through the horizontal plane of Re atoms reveal the localization of electrons with an approximate $ELF$ value of 0.5 between the Re chains in *[4 F@Above A]* (Figure 11(d)). As a comparison, when the F atoms are adsorbed between Re chains (*[4 F@Bet]*, Figure 11(e)), the $ELF$ is lower at around 0.2. These suggest that ionic interaction exists between Re atoms in neighboring chains, and the depletion of these electrons between Re chains occurs if F atoms are adsorbed above the regions between the chains. The negative Laplacian plots complement the $ELF$ plots; the bond critical points (bcp) between the Re chains have a negative Laplacian value of about -1.8 (in green), indicating the ionic, but non-trivial nature of the interaction between the

chains (Figures 11(f) and (g)). However it is not evident from the plots that the ionicity is reduced in (*[4 F@Bet]*, as shown in Figure 11(e). Moreover, the bonds between Re atoms within the chains are more covalent in comparison, since the bcp has a negative Laplacian value of about -0.2 (in red).

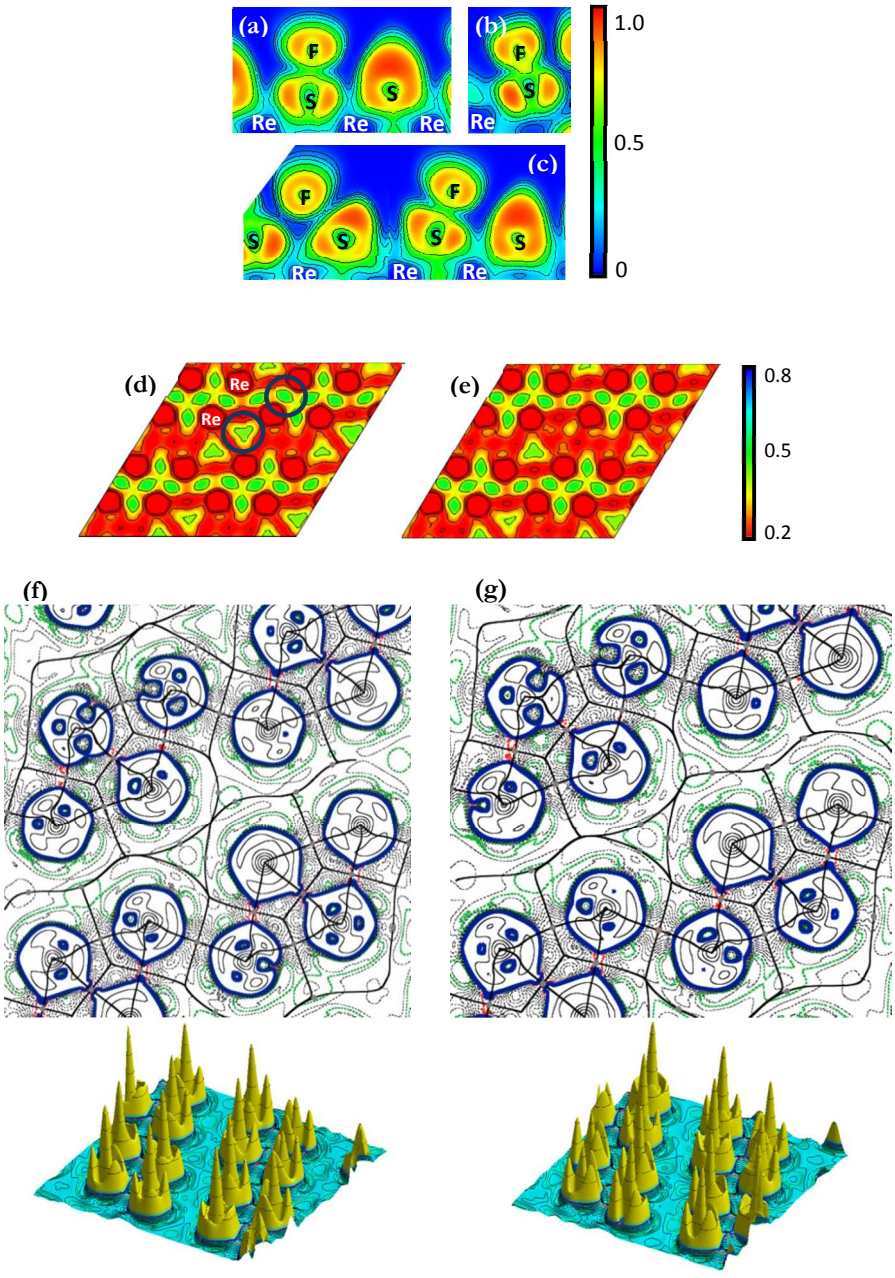

*Figure 11. Electron localization landscape in the plane formed by F atom and neighboring atoms - (a) [4 F@Above A], (b) [4 F@Above B], and (c) [4F@Bet](d). Through Re atoms - (d) [4 F@Above A], and (e) [4F@Bet]. The color bars show the dimensionless electron localization values. 2D (top) and 3D (bottom) negative Laplacian plots through Re atoms: (f) [4 F@Above A], and (g) [4 F@Above B]. The green and red dashed lines in the 2D negative Laplacian plots denote the contour lines with values of -1.8 and -0.2, respectively.*

## 4. Summary

$ReS_2$, a member of the transition metal dichalcogenide family, has a unique distorted orthogonal structure. Due to its geometrical distortion, layers in its bulk form are decoupled electronically and vibrationally, i.e. layer dependence of its properties is diminished. Since functionalization of a material with F atoms is one of the many ways to alter its electronic and magnetic properties, we employ density functional theory to investigate the effects of fluorination on $ReS_2$. Comparison is made between fluorination at sites above and between Re chains. Fluorinating the Re chains at either Position A or B induces metallic mid-gap states, while fluorinating the regions between Re chains induces semiconducting mid-gap states. The orbital-projected band structure and the band-decomposed charge density show that the metallic mid-gap states originate from F-$p_z$, Re-$d_{xz}$, and S-$p_z$ electrons, while the semiconducting counterparts are associated with Re-$d_{xy}$, Re-$d_{x2}$, S-$p_z$, and F-$p_z$ states. The metallic mid-gap states are FM-coupled within the chain, and AFM-coupled between chains. On the other hand, the semiconducting mid-gap states are non-magnetic. The disparity of the electronic and magnetic character between both types of mid-gap states suggests a strong role played by the coupling between the Re and F atoms. The mid-gap states induced by fluorination at Position A above the Re chains are relatively more robust to electric field effects. Essentially, the formation of

these localized mid-gap states implies that hopping conduction of the states is possible along the Re chain. Last but not least, ***ELF*** and negative Laplacian plots show that the F-S bonds have a strong ionic character. Interestingly, Re atoms in neighboring chains interact ionically, and the interaction is reduced when F atoms are adsorbed above the regions between the Re chains.

## ACKNOWLEDGEMENTS

G.C.L. gratefully acknowledges A*STAR for funding under the A*STAR International Fellowship (2013-2015). The computations were performed on the MTU Superior cluster, and support from Dr. S. Gowtham is appreciated.

## ASSOCIATED CONTENT

Supporting Information

Vibrational frequencies. *[4 F@Above A]:* Initial AFM spin configurations. Spin-polarized atomic-projected band structure.

## AUTHOR INFORMATION

Corresponding Authors

*(G. C. L.) E-mail: jgloh@mtu.edu

*(R. P.) E-mail: pandey@mtu.edu

Notes

The authors declare no competing financial interest.

## REFERENCES

(1) Novoselov, K. S.; Jiang, D.; Schedin, F.; Booth, T. J.; Khotkevich, V. V.; Morozov, S. V.; Geim, A. K. Two-dimensional atomic crystals. *Proc. Nat. Acad. Sci.* **2005**, *102*, 10451-10453.

(2) Kane, C. L.; Mele, E. J. Quantum spin hall effect in graphene. *Phys. Rev. Lett.* **2005**, *95*, 226801.

(3) Beenakker, C. W. J. Specular Andreev reflection in graphene. *Phys. Rev. Lett.* **2006**, *97*, 067007.

(4) McCann, E.; Kechedzhi, K.; Fal'ko, V. I.; Suzuura, H.; Ando, T.; Altshuler, B. L. Weak-localization magnetoresistance and valley symmetry in graphene. *Phys. Rev. Lett.* **2006**, *97*, 146805.

(5) Titov, M.; Beenakker, C. W. J. Josephson effect in ballistic graphene. *Phys. Rev. B* **2006**, *74*, 041401(R).

(6) Nomura, K.; MacDonald, A. H. Quantum transport of massless Dirac fermions. *Phys. Rev. Lett.* **2007**, *98*, 076602.

(7) Somoano, R. B.; Hadek, V.; Rembaum, A. Alkali-metal intercalates of molybdenum disulfide. *J. Chem. Phys.* **1973**, *58*, 697-701.

(8) Farr, J. P. G. Molybdenum-disulfide in lubrication – review. *Wear* **1975**, *35*, 1-22.

(9) Baugher, B. W. H.; Churchill, H. O. H.; Yang, Y.; Jarillo-Herroro, P. Intrinsic electronic transport properties of high-quality monolayer and bilayer $MoS_2$. *Nano Lett.* **2013**,*13*, 4212-4216.

(10) Lembke, D.; Kis, A. Breakdown of high-performance monolayer $MoS_2$ transistors. *ACS Nano* **2012**, *6*, 10070-10075.

**(11)** Braga, D.; Gutiérrez Lezama, I.; Berger, H.; Morpurgo, A. F. Quantitative determination of the band gap of $WS_2$ with ambipolar ionic liquid-gated transistors. *Nano Lett.* **2012**, *12*, 5218-5223.

**(12)** Fang, H.; Chuang, S.; Chang, T. C.; Takei, K.; Takahashi, T.; Javey, A. High-performance single layered $WSe_2$ p-FETs with chemically doped contacts. *Nano Lett.* **2012**, *12*, 3788-3792.

**(13)** Ataca, C.; Şahin, H.; Ciraci, S. Stable, single-layer $MX_2$ transition-metal oxides and dichalcogenides in a honeycomb-like structure. *J. Phys. Chem. C* **2012**, *116*, 8933-8999.

**(14)** Gordon, R. A.; Yang, D.; Crozier, E. D.; Jiang, D. T.; Frindt, R. F. Structures of exfoliated single layers of $WS_2$, $MoS_2$, and $MoSe_2$ in aqueous suspension. *Phys. Rev. B* **2002**, *65*, 125407.

**(15)** Wang, Q. H.; Kalantar-Zadeh, K.; Ki, A.; Coleman, J. N.; Strano, M. S. Electronics and optoelectronics of two-dimensional transition metal dischalcogenides. *Nat. Nanotechnol.* **2012**, *7*, 699-712.

**(16)** Mak, K. F.; Lee, C.; Hone, J.; Shan, J.; Heinz, T. F. Atomically thin $MoS_2$: a new direct-gap semiconductor. *Phys. Rev. Lett.* **2010**, *105*, 136805.

**(17)** Han, S. W.; Kwon, H.; Kim, S. K.; Ryu, S.; Yun, W. S.; Kim, D. H.; Hwang, J. H.; Kang, J. –S.; Baik, J.; Shin, H. J. et al. Band-gap transition induced by interlayer van der Waals interaction in $MoS_2$. *Phys. Rev. B* **2011**, *84*, 045409.

**(18)** Ellis, J. K.; Lucero, M. J.; Scuseria, G. E. The indirect to direct band gap transition in multilayered $MoS_2$ as predicted by screened hybrid density functional theory. *Appl. Phys. Lett.* **1011**, *99*, 261908.

**(19)** Neville, R. A.; Evans, B. L. Band edge excitons in 2H-$MoS_2$. *Phys. Stat. Sol. B* **1976**, *73*, 597-606.

**(20)** Horzum, S.; Sahin, H.; Cahangirov, S.; Cudazzo, P.; Rubio, A.; Serin, T.; Peeters, F. M. Phonon softening and direct to indirect band gap crossover in strained single-layer $MoSe_2$. *Phys. Rev. B* **2013**, *87*, 125415.

**(21)** Sahin, H.; Tongay, S.; Horzum S.; Fan, W.; Zhou, J.; Li, J.; Wu, J.; Peeters, F. M. Anomalous Raman spectra and thickness-dependent electronic properties of $WSe_2$. *Phys. Rev. B* **2013**, *87*, 165409.

**(22)** Wilson, J. A.; DiSalvo, F. J.; Mahajan, S. Charge-density waves and superlattices in the metallic layered transition metal dichalcogenides. *Adv. Phys.* **1975**, *24*, 117.

**(23)** Tongay, S.; Sahin, H.; Ko, C.; Luce, A.; Fan, W.; Liu, K.; Zhou, J.; Huang, Y. –S.; Ho, C. –H.; Yan, J. Monolayer behaviour in bulk $ReS_2$ due to electronic and vibrational decoupling. *Nat. Commun.* **2014**, *5*, 1-6.

**(24)** Fujita, T.; Ito, Y.; Tan, Y.; Yamaguchi, H.; Hojo, D.; Hirata, A.; Voiry, D.; Chhowalla, M.; Chen, M. Chemically exfoliated $ReS_2$ nanosheets. *Nanoscale* **2014**, *6*, 12458-12462.

**(25)** Corbet, C. M.; McClellan, C.; Rai, A.; Sonde, S. S.; Tutuc, E.; Banerjee, S. K. Field effect transistors with current saturation and voltage gain in ultrathin ReS2. *ACS Nano* **2015**, *9*, 363-370.

**(26)** Doni, E.; Girlanda, R. *Electronic structure and electronic transitions in layered materials*; Springer-Verlag: Berlin, 1986.

**(27)** Liu, L.; Feng, Y. P.; Shen, Z. X. Structural and electronic properties of *h*-BN. *Phys. Rev. B* **2003**, *68*, 104102.

**(28)** Constantinescu, G.; Kuc, A.; Heine, T. Stacking in bulk and bilayer hexagonal boron nitride. *Phys. Rev. Lett.* **2013**, *111*, 036104.

**(29)** Friemelt, K.; Kulikova, L.; Kulyuk, L.; Siminel, A.; Arushanov, E.; Kloc. Ch.; Bucher, E. Optical and photoelectrical properties of $ReS_2$ single crystals. *J. Appl. Phys.* **1996**, *79*, 9268.

**(30)** Andriotis, A. N. Tunable magnetic properties of transition metal doped $MoS_2$. *Phys. Rev. B* **2014**, *90*, 125304.

**(31)** Ouyang, F.; Yang, Z.; Ni, X.; Wu, N.; Chen, Y.; Xiong, X. Hydrogenation-induced edge magnetization in armchair $MoS_2$ nanoribbon and electric field effects. *Appl. Phys. Lett.* **2014**, *104*, 071901.

**(32)** Ouyang, F.; Ni, X.; Yang, Z.; Chen, Y.; Zheng, X.; Xiong, X. Effects of edge hydrogenation on structural stability, electronic, and magnetic properties of $WS_2$ nanoribbons. *J. Appl. Phys.* **2013**, *114*, 213701.

**(33)** Kim, H. –J.; Cho, J. –H. Fluorine-induced local magnetic moment in graphene: a hybrid DFT study. *Phys. Rev. B* **2013**, *87*, 174435.

**(34)** Zhou, J.; Wang, Q.; Sun, Q.; Jena, P. Electronic and magnetic properties of a BN sheet decorated with hydrogen and fluorine. *Phys. Rev. B* **2010**, *81*, 085442.

**(35)** Feng, Y.; Zhou, W.; Wang, Y.; Zhou, J.; Liu, E.; Fu, Y.; Ni, Z.; Wu, X.; Yuan, H.; Miao, F. et al. Raman vibrational spectra of bulk to monolayer $ReS_2$ with lower symmetry. **arxiv.org/abs/1502.02835.**

**(36)** Kresse, G.; Joubert, D. From ultrasoft pseudopotentials to the projector augmented-wave method. *Phys. Rev. B* **1999**, *59*, 1758.

**(37)** Perdew, J. P.; Burke, K.; Ernzerhof, M. Generalized gradient approximation made simple. *Phys. Rev. Lett.* **1996**, *77*, 3865.

**(38)** Grimme, S.; Anthony, J.; Ehrlich, S.; Krieg, S. A consistent and accurate ab initio parametrization of density functional dispersion correction (dft-d) for the 94 elements H-Pu. *J. Chem. Phys.* **2010**, *132*, 154104.

**(39)** Monkhorst, H. J.; Pack, J. D. Special points for Brillouin-zone integrations. *Phys. Rev. B* **1976**, *13*, 5188.

**(40)** Hellmann, H. *Einführung in die quantenchemie*; Leipzig, 1937.

**(41)** Feynman, R. P. Forces in molecules. *Phys. Rev.* **1939**, *56*, 340.

**(42)** Bader, R. F. W. *Atoms in molecules. A quantum theory*; Clarendon Press: Oxford, 1994.

**(43)** Bader, R. F. W. Atoms in molecules. *Acc. Chem. Res.* **1985**, *18*, 9-15.

**(44)** Bader, R. F. W. A quantum theory of molecular structure and its applications. *Chem. Rev.* **1991**, *91*, 893-928.

**(45)** Sagar, R. P.; Ku, A. C. T.; Smith, V. H. Jr.; Simas, A. M. The Laplacian of the charge density and its relationship to the shell structure of atoms and ions. *J. Chem. Phys.* **1988**, *88*, 4367.

**(46)** Shi, Z.; Boyd, R. J. The shell structure of atoms and the Laplacian of the charge density. *J. Chem. Phys.* **1988**, *88*, 4375.

**(47)** Horzum, S.; Çakir, D.; Suh, J.; Tongay, S.; Huang, Y. –S.; Ho, C. –H.; Wu, J.; Sahin, H.; Peeters, F. M. Formation and stability of point defects in monolayer rhenium disulphide. *Phys. Rev. B* **2014**, *89*, 155433.

**(48)** Pauling, L. Atomic radii and interatomic distances in metals. *J. Am. Chem. Soc.* **1947**, *69*, 542-553.

**(49)** Miyazaki, H.; Tsukagoshi, K.; Kanda, A.; Otani, M.; Okada, S. Influence of disorder on conductance in bilayer graphene under perpendicular electric field. *Nano Lett.* **2010**, *10*, 3888-3892.

**(50)** Zou, K.; Zhu, J. Transport in gapped bilayer graphene: the role of potential fluctuations. *Phys. Rev. B* **2010**, *82*, 081407 (R).

**(51)** Taychatanapat, T.; Jarillo-Herrero, P. Electronic transport in dual-gated bilayer graphene at large displacement fields. *Phys. Rev. Lett.* **2010**, *105*, 166601.

**(52)** Oostinga, J. B.; Heersche, H. B.; Liu X.; Morpurgo, A. F.; Vandersypen, L. M. K. Gate-induced insulating state in bilayer graphene devices. *Nature Mater.* **2007**, *7*, 151-157.

**(53)** Jing, L.; Velasco Jr, J.; Kratz, P.; Liu, G.; Bao, W.; Bockrath, M.; Lau, C. N. Quantum transport and field-induced insulating states in bilayer graphene pnp junctions. *Nano Lett.* **2010**, *10*, 4000-4004.

**(54)** Yan, J.; Fuhrer, M. S. Charge transport in dual gated bilayer graphene with Corbino geometry. *Nano Lett.* **2010**, *10*, 4521-4525.

**(55)** Young, A. F.; Dean, C. R.; Sorgenfrei, M. S.; Ren, H.; Watanabe, K.; Taniguchi, T.; Hone, J.; Shepard, K. L.; Kim, P. Electronic compressibility of layer-polarized bilayer graphene. *Phys. Rev. B* **2012**, *85*, 235458.

**(56)** Rossi, E.; Das Sarma, S. Inhomogenous electronic structure, transport gap, and percolation threshold in disordered bilayer graphene. *Phys. Rev. Lett.* **2011**, *107*, 155502.

**(57)** Han, J.; Shen, M.; Cao, W.; Senos, A. M. R.; Mantas, P. Q. Hopping conduction in Mn-doped ZnO. *Appl. Phys. Lett.* **2003**, *82*, 67-69.

**(58)** Savin, A.; Nesper, R.; Wengert, S.; Fässler, T. F. ELF: The electron localization function. *Angew. Chem. Int. Ed. Engl.* **1997**, *36*, 1808-1832.

**(59)** Poater, J.; Duran, M.; Solà, M.; Silvi, B. Theoretical evaluation of electron delocalization in aromatic molecules by means of atoms in molecules (AIM) and electron localization function (ELF) topological approaches. *Chem. Rev.* **2005**, *105*, 3911-3947.

**(60)** Alikhani, M. E.; Fuster, F.; Silvi, B. What can tell the topological analysis of ELF on hydrogen bonding. *Structural Chem.* **2005**, *16*, 203-210.

**(61)** Becke, A. D.; Edgecombe, K. E. A simple measure of electron localization in atomic and molecular systems. *J. Chem. Phys.* **1990**, *92*, 5397.

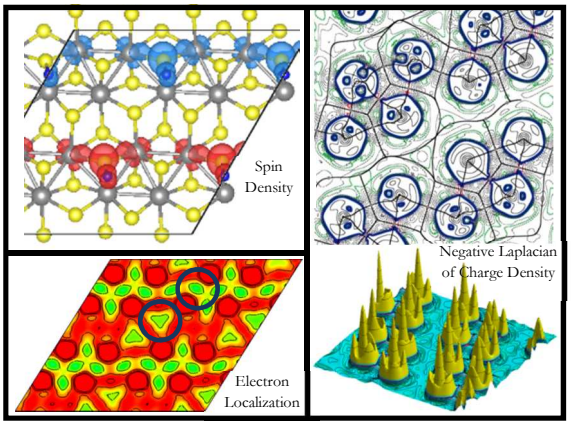


TOC Graphic